# LES STUDY ON THE LARGE-SCALE MOTIONS OF WALL TURBULENCE AND THEIR STRUCTURAL DIFFERENCE BETWEEN PLANE CHANNEL AND PIPE FLOWS

**Makoto Tsubokura**
Department of Mechanical Engineering and Intelligent Systems,
The University of Electro-Communications
Chofu-shi, Tokyo 182-8585, Japan
tsubo@mce.uec.ac.jp

## ABSTRACT

The large-scale motions of wall turbulence are investigated numerically using the large eddy simulation (LES) technique. Special attention is paid to how geometrical difference affects the large structures. For this purpose LES of plane channel and pipe flows ($Re_\tau = 395, 590, 1180$) using a large analysis region is conducted. It is found that in the outer layer, the spanwise/azimuthal spacing of the large scales is stable at 1.4 times the boundary layer thickness (roughly the same as the channel half-width or the radius of pipe). Thus, the number of the large motions allocating along the spanwise direction remains the same throughout the outer layer of channel flow, while its number in the pipe along the azimuthal direction changes stepwise against the wall distance. Consequently strong interaction among the large motions occurs in pipe flow and the streamwise size of the large scales are slightly smaller in pipe (2 to 4 times the radius) than those in channel (3 to 5 times the half-height). The very large scales in the log layer remarkably appear at higher Reynolds number case of both channel and pipe flows are also noteworthy.

## INTRODUCTION

It has been widely acknowledged that in wall turbulence there exist large-scale structures of a size at least comparable to the boundary layer thickness. In contrast to the small-scale structures near the wall, less attention has been paid to the large structures until recently. However, owing to the recent study on the structures of high Reynolds-number turbulence and their $Re$ scaling, the outer large structures and especially their interaction with the small scales near the wall appears to be an important issue in the understanding of wall turbulence. In fact, the $Re$ dependence of the streamwise velocity fluctuations near the wall could be explained as a contribution of the outer motions to the inner structures, and evidence of this idea has been shown, for example, by DeGraaff & Eaton (2000), in which they successfully discovered that the streamwise velocity rms collapses well in inner-outer mixed scaling.

The existence of the large scales has been recognized on the experimental data of turbulent pipe flow, which indicate an abnormal extent of the temporal auto correlation appearing only in the streamwise velocity component, or the low wavenumber peak of the corresponding premultiplied one-dimensional (1-D) power spectra (Kim & Adrian, 1999). However, the one-point measurements most frequently used in experimental studies have fundamental difficulty in describing the spatial characteristics of large-scale structures.

On the other hand, rapid growth of recent high-performance computers makes it possible to apply DNS to investigate the large structures of wall-turbulence (*e.g.*, Del Álamo & Jiménez, 2001). They adopted the plane turbulent channel flow as an analysis model and studied the spatial features of the large structures. It is true that the turbulent channel flow is an ideal case and has a universal feature of wall turbulence. But we should concern ourselves with the difference of the large structures between plane and pipe flows when we compare our numerical results with the abundant experimental results of pipe flows. The typical case with regard to this matter may be relating to the $k_x^{-1}$ region ($\phi_{uu} \propto k_x^{-1}$ ) in the streamwise premultiplied $u$-spectra, which should appear as a plateau if the region exists. This $k_x^{-1}$ region was explained as a self-similar structure obtained by a simple scaling concept in the context of Townsend's attached-eddy hypothesis (Perry *et al.*, 1986). While this idea has been supported by much experimental data in the fully developed pipe flow (e.g., Kim & Adrian, 1999 and Perry *et al.*, 1986) and is widely accepted, recent measurements of a pipe by Morrison *et al.* (2002) at a very high $Re$ contradict it. Concerning this matter, Del Álamo & Jiménez (2001) reported that their DNS results of the plane channel flow also do not show the $k_x^{-1}$ region.

The objective of this study is to investigate the large scale structures of wall-turbulence typically appear in outer layer in the context of their $Re$ scaling and interaction with the buffer layer turbulence. In the present work, we especially focus on how geometrical difference affects their outer-layer motions. The practical difficulty of studying the large-scale structures lies in the fact that they require a large experimental setup or a computational domain at sufficiently high $Re$ conditions in order to properly capture their entire motions, and this requirement has been the stumbling block to both experiments and DNS for large-scale studies. Alternatively we have adopted large eddy simulation (LES) as an analysis tool, which will be a promising method because we can save much computational resources to be consumed for the dissipative small eddies.

## NUMERICAL METHODS

### Analysis Models

The analysis models adopted in this study are the plane channel with the half-height of $\delta$ and pipe with the radius of $R$, both of which have the sufficiently long analysis region of $8\pi\delta$ and $8\pi R$, respectively, to capture the large scale motions

in the outer layer. The streamwise direction is supposed to be periodic, and constant pressure gradient is imposed to obtain statistically steady state. A periodic boundary condition is also imposed in the spanwise direction of the plane channel. Hereafter, $x$, $y$, and $z$ indicate the streamwise, normal-wall, and spanwise/azimuthal directions, respectively.

### Governing Equations

The governing equations for the present work are obtained from the incompressible Navier-Stokes equations, which is nondimensionalized by the reference length, $\delta$ or $R$, and velocity $u_\tau = \sqrt{\tau_w}$ (the friction velocity) so as to make the mean pressure gradient force as 1, and the following nondimensional filtered continuity and momentum equations written in the Cartesian coordinates are obtained:

$$\frac{\partial \bar{u}_i}{\partial x_i} = 0, \tag{1}$$

$$\frac{\partial \bar{u}_i}{\partial t} + \frac{\partial \bar{u}_i \bar{u}_j}{\partial x_j} = -\frac{\partial \bar{p}}{\partial x_i} + \frac{1}{Re_\tau}\frac{\partial^2 \bar{u}_i}{\partial x_j \partial x_j} + \delta_{i1} - \frac{\partial}{\partial x_j}\tau_{ij}, \tag{2}$$

in which an *overbar* denotes the *grid* filtering operation, and indices $i = 1, 2$, and 3 represent the directions for $x, y$, and $z$, respectively. Here, $\bar{u}_i$ is the grid-scale (GS) or resolved velocity, $\bar{p}$ is the GS pressure divided by the constant density, and $Re_\tau$ is the friction Reynolds number given as $u_\tau \delta/\nu$. The last term of eq. (2) is the subgrid-scale (SGS) stress term, which must be modeled. For pipe flow, the corresponding equations written in the cylindrical coordinates are used, and the friction Reynolds number is given as $Re_\tau = u_\tau R/\nu$.

### Discretization

We have adopted the fully conservative high-order FD scheme for uniform Cartesian staggered grids by Morinishi *et al.* (1998) and the extension of the method to the non-uniform grids in cylindrical coordinates (Morinishi *et al.*, 2004). All spatial derivatives are discretized by the fourth-order FD, except for the SGS term which is discretized by the second-order.

The third-order Runge-Kutta scheme is adopted as the time marching method, except for the second derivative for the normal-wall direction included in the viscous term, which is treated semi-implicitly using the Crank-Nicolson method for the tolerance of the time increment in the numerical simulation. The fractional step method (Dukowicz & Dvinsky, 1992) is used for the velocity-pressure coupling and the corresponding Poisson equation for pressure is solved by the Fast Fourier Transform method in the periodic directions while the septa-diagonal method is used in the normal-wall direction. For details of the discretization method, refer to Morinishi *et al.* (1998, 2004)

### Subgrid-scale Modeling

An isotropic eddy viscosity model developed previously by Tsubokura (2001) for the dynamic procedure (Germano *et al.*, 1991) using FD method is adopted in this study, in which the SGS stress and the corresponding *subtest*-scale (STS) stress, $T_{ij} = \widetilde{\overline{u_i u_j}} - \tilde{\bar{u}}_i \tilde{\bar{u}}_j$, are modeled as follows:

$$\tau_{ij} - \frac{1}{3}\delta_{ij}\tau_{kk} = -2C\frac{k}{3|\bar{S}|}\bar{S}_{ij}, \tag{3}$$

$$T_{ij} - \frac{1}{3}\delta_{ij}T_{kk} = -2C\frac{K}{3|\tilde{\bar{S}}|}\tilde{\bar{S}}_{ij}, \tag{4}$$

Table 1: Numerical conditions of the plane channels for the grid-resolution test: LES, $Re_\tau = 590$; DNS, $Re_\tau = 550$.

| *cases* | *Domain size* | *Grid number* | *Grid spacing* | |
|---|---|---|---|---|
| | $L_x/\delta \times L_z/\delta$ | $N_x \times N_z$ | $h_x^+$ | $h_z^+$ |
| (I) | $8\pi \times 4\pi$ | $192 \times 192$ | 77.2 | 38.6 |
| (II) | $8\pi \times 4\pi$ | $256 \times 256$ | 57.9 | 29.0 |
| (III) | $8\pi \times 4\pi$ | $384 \times 384$ | 38.6 | 19.3 |
| (IV) | $8\pi \times 4\pi$ | $512 \times 512$ | 29.0 | 14.5 |
| (V) | $8\pi \times 4\pi$ | $512 \times 384$ | 29.0 | 19.3 |
| DNS | $8\pi \times 4\pi$ | $1536 \times 1536$ | 8.9 | 4.5 |

where $S_{ij}$ is the strain rate tensor, $S$ is its magnitude given as $S = \sqrt{2S_{ij}S_{ij}}$, and an *over-tilde* denotes the *test* filtering operation. The $k$ and $K$ in (1) and (2) are the SGS and STS turbulence energy, and are modeled by the scale similarity concept as follows: $k = \overline{\bar{u}_k \bar{u}_k} - \bar{\bar{u}}_k \bar{\bar{u}}_k$, $K = \widetilde{\overline{\tilde{\bar{u}}_k \tilde{\bar{u}}_k}} - \tilde{\tilde{\bar{u}}}_k \tilde{\tilde{\bar{u}}}_k$, which was determined considering the consistency of the numerical error in the dynamic procedure. In order to avoid any instability induced by possible negative eddy viscosity through negative $C$, an averaging technique proposed in the original procedure is adopted in the homogeneous directions.

### Determination of Grid Resolutions

As a preliminary test of the large scale study, we focus on the minimum grid resolution required for the reproduction of large scales in fully developed incompressible turbulent plane channel flow. Because the size of the large scales in the outer layer are comparable to the boundary layer thickness, it is expected that relatively coarse grids will be sufficient to resolve their motions, based on the assumption that their outer motions are detached from the wall and self-organized. On the other hand, if they originate from the small organized structures in the vicinity of the wall, the grids required for large scales will be unexpectedly fine enough to reproduce the near-wall dominant motions.

A moderate friction Reynolds number of 590 is adopted at which reliable DNS data are provided by Del Álamo & Jiménez (2003) ($Re_\tau = 550$). It is acknowledged in their DNS that the large scale motions obtain substantial energy only in the streamwise velocity component. Thus we focus on the ability of LES in regard to how properly it can reproduce the premultiplied power spectra of the streamwise velocity fluctuations at various grid resolutions indicated as (I) to (V) in Table 1. At least 5 grid points are allocated through the viscous sublayer to capture the rapid growth of the mean velocity in the vicinity of the wall, and total of 65 grid points are used for the normal-wall direction ($h_y^+ = 1.6 \sim 44.9$) in all LES tested here, while 257 grid points are used in the DNS ($h_y^+ < 6.7$). Special attention is paid to a low-wavenumber feature of the spectra in the outer layer where the large scales remarkably appear. In all cases, the adopted domain size is the same as that of DNS, and the only difference among each LES is the grid resolution for the streamwise and spanwise directions. The one-dimensional premultiplied power spectra of the streamwise velocity component are shown in Fig. 1. Before focusing on the outer-layer in which large scales are remarkably observed, let us first discuss the near-wall spectra at $y^+ \sim 20$ where the well-known buffer-layer streaks appear

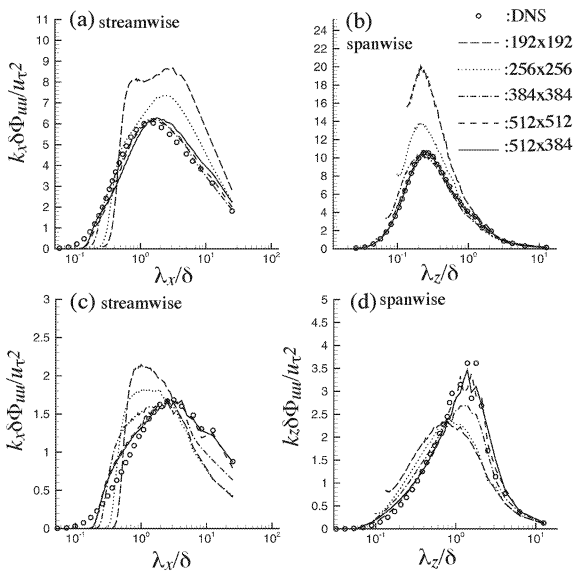


Figure 1: The 1-D premultiplied power spectra of the streamwise velocity of *plane channel* flows: (a) & (b), near wall at $y^+ \sim 20$; (b) & (d), away from the wall at $y^+ \sim 200$ .

and the maximum rms of the streamwise velocity tends to be located. The premultiplied spectra obtained by the DNS peak at $\lambda_x\delta = 1.48$ and $\lambda_z\delta = 0.23$ as seen in Figs. 1(a) and (b). These values are equivalent to $\lambda_x^+ \sim 810$ and $\lambda_z^+ \sim 130$ in inner scaling, which represents the scales of the buffer-layer streaks for streamwise and spanwise direction respectively. Unfortunately, the actual LES of coarser grids such as (I) and (II) fails to reproduce the spectral feature of DNS in the resolved range and cutoff SGS energy seems to pile up on the resolved scale. From these results, it seems that the grid spacing of at least $h_x^+ \sim 30$ and $h_z^+ \sim 20$ used in (V) is indispensable to properly capture the near-wall spectral feature. We now look at the outer-layer spectra ($y^+ \sim 200$) with the object of the reproduction of the large scales. The DNS spectra peaks at $\lambda_x\delta \sim 2.7$ and $\lambda_z\delta \sim 1.8, .14$ in outer scaling, as seen in Figs. 1(c) and (d). These low-wavenumber energetic modes represent the characteristic sizes of the large scales. Contrary to the optimistic expectation that rather coarser grids such as (I) and (II), which failed to capture the small scales near the wall, might be sufficient to reproduce the large scales in this region, we see that they again fail to reproduce the GS spectra and that they provide an underestimation of the peak wavelength. Reproduction of the steep peak observed in DNS in the spanwise spectrum is also unsatisfactory and only the moderate peak can be identified at the lower wavelength than the DNS value. This poor performance of the coarse LES was improved by increasing the grid resolution, and (IV) and (V) are both qualitatively and quantitatively accurate enough to reproduce the DNS spectra.

According to the results in the context of the reproduction of the peak spectra shown above, we can say that at least the grid resolution corresponding to (V) is necessary for the analysis of the large scales. The plausible explanation of the requirement of the surprisingly fine grid resolution compared with the characteristic sizes of the large scales is that the large scales originate from the near-wall motions related to the sublayer streaks. Practically speaking, this grid resolution is relatively fine considering the engineering or geophysical applications of LES, but the total grid number of LES is still about one-fiftieth of that used in the referenced spectral DNS, and the advantage of LES for studying the large scales is still maintained.

Table 2: Numerical conditions for plane channel and pipe flows:.

| *geometry* | $Re_\tau$ | *Domain size* $L_x \times L_y \times L_z$ | *Grid number* $N_x \times N_y \times N_z$ |
|---|---|---|---|
| plane | 395 | $8\pi\delta \times 2\delta \times 4\pi\delta$ | $360 \times 45 \times 256$ |
| | 590 | $8\pi\delta \times 2\delta \times 4\pi\delta$ | $512 \times 65 \times 384$ |
| | 1180 | $8\pi\delta \times 2\delta \times 2.25\pi\delta$ | $1024 \times 129 \times 432$ |
| pipe | 395 | $8\pi R \times R \times 2\pi$ | $360 \times 23 \times 256$ |
| | 590 | $8\pi R \times R \times 2\pi$ | $512 \times 33 \times 384$ |
| | 1180 | $8\pi R \times R \times 2\pi$ | $1024 \times 65 \times 432$ |

## RESULTS

In accordance with the required minimum grid resolution, $h_x^+ \sim 30$ and $h_z^+ \sim 20$, found in the previous section, LES of plane channel and pipe flows at three $Re_\tau$ of 395, 590, and 1180 are conducted. The domain size and the adopted grid number are summarized in table 2.

### Turbulence Statistics

Figure 2 indicates the streamwise mean velocity obtained by our LES at (*a*)$Re_\tau = 590$ and (b)1180 in *inner* scaling ($u_\tau$ and $\nu$); for reference, the laws of the wall, $U^+ = y^+$ and $U^+ = (1/0.41)\ln y^+ + 5.2$, as well as the DNS data (the plane channel at $Re_\tau = 550$) obtained by Del Álamo & Jiménez (2003), is also plotted. We cannot observe a significant difference at the logarithmic layer between plane and channel flows, while remarkable difference appears on the upper side of the outer layer ($y/\delta$ or $y/R > 0.2$, equivalent to $y^+ > 120$ at $Re_\tau = 590$ and $y^+ > 240$ at $Re_\tau = 1180$). This difference is more remarkable when plotted in *outer* scaling ($u_\tau$, and $\delta$ or $R$), which is often called the *velocity-defect law*. Correspondingly, the turbulent intensity profiles also show the similar tendency; the difference is observed above $y/\delta$ or $y/R = 0.2$.

### 1-D Premultiplied Spectra

One-dimensional premultiplied power spectra of the

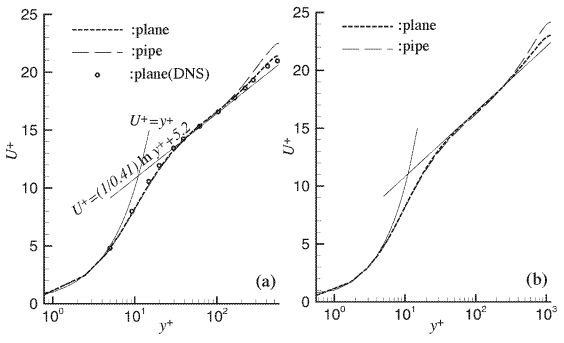


Figure 2: Mean velocity profiles: (a), $Re_\tau = 590$; (b), $Re_\tau = 1180$.

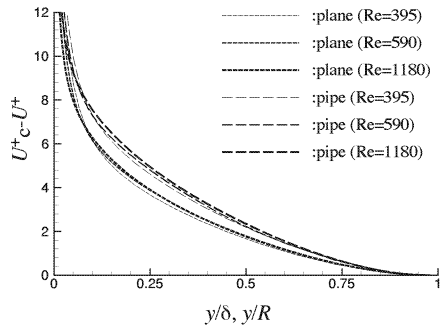


Figure 3: Mean velocity defect.

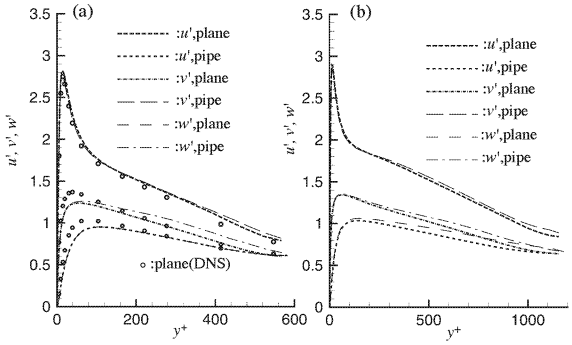


Figure 4: Turbulent intensity profiles: (a), $Re_\tau = 590$; (b), $Re_\tau = 1180$.

streamwise velocity component obtained in plane channel and pipe flows are plotted in Fig. 5 (near wall) and 6 (away from the wall). Note that the power spectrum multiplied by the wave number $k\phi_{uu}$ in the logarithmic plot indicates that the area under the profile is proportional to the power or energy included in the corresponding wavenumber range. Figure 5 shows that the spectral tendency is the same for each geometrical configuration near the wall, while notable difference appears in or above the logarithmic layer. As indicated in Fig. 6(a), both the plane channel and pipe show a peak at the second largest mode ($\lambda_x/\delta = 4\pi$) at $y^+ \sim 200$, which indicates the typical size of the large scale motions. In case of the pipe, this energetic mode is mitigated above the logarithmic layer ($y^+ > 400$), while the channel maintains this spectral peak even in the wake region. These figures clearly suggest that near-wall organized structures are essentially the same between the plane channel and pipe, while outer large scales are different between them. It also should be mentioned that the peak at the second largest mode suggests that the numerical box for streamwise direction at the log layer is not sufficiently large enough to capture the streamwise largest motions and slightly larger structures might exist there.

## SNAPSHOTS

Figures 7 and 8 indicate the grey-scale coded contours of instantaneous streamwise velocity fluctuations obtained in plane channel and pipe flows at $Re_\tau = 1180$. We can observe on the plane at $y^+ \sim 200$ the coherent streaky structures similar to the low-speed streaks in the near-wall region. However, their spanwise spacing is equivalent to the order of the channel

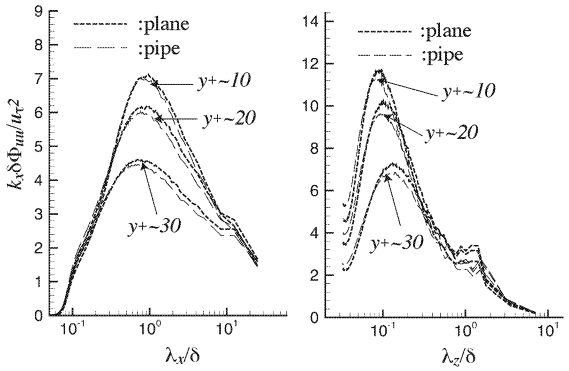


Figure 5: 1-D premultiplied power spectra of the streamwise velocity ($y^+ \sim 20$) at $Re_\tau = 1180$: (a), streamwise; (b), spanwise or azimuthal.

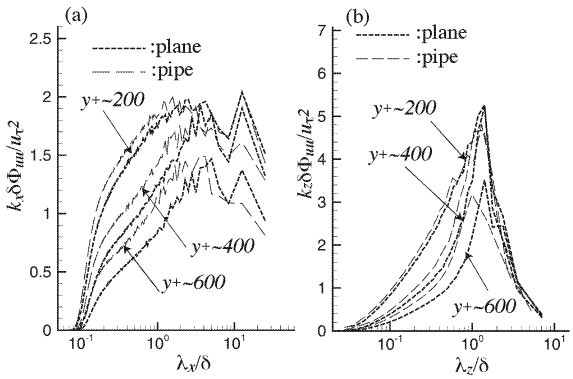


Figure 6: 1-D premultiplied power spectra of the streamwise velocity ($y^+ \sim 200$) at $Re_\tau = 1180$: (a), streamwise; (b), spanwise or azimuthal.

height or the pipe radius. Figure. 8 also shows that the large lower-velocity zones (appearing as the large dark spots) align in the spanwise and azimuthal directions, and compared with the low-speed streaks appearing as very small black dots in the vicinity of the wall, their size are remarkably large. It is also evident that the large scales penetrate deep into the near-wall region, which affects the characteristics of the near-wall region. The possible explanation of this deep penetration of the large scale is its contribution of the $Re$-number dependence of the rms of the streamwise velocity near the wall. The most notable difference of these large lower-velocity zones between plane and pipe flows are that , owing to the confined geometry of the pipe toward the pole, each large structure in the pipe seems to be interact with each other near the pole. As a result of this interaction, the size of the large structures in the pipe are seemingly slightly smaller than the ones observed in the plane channel flow, as shown in Fig. 7 ($y^+ \sim 200$)

## SCALING OF THE ENERGETIC MODES

The most energetic wavelengths of plane channel and pipe flows, at which the peak of the 1-D premultiplied spectra of the streamwise velocity are located, are plotted in Figs. $9 \sim 12$ against the distance from the wall to investigate the characteristic size of the turbulence structures, and their dependences on the flow geometry and Reynolds number.

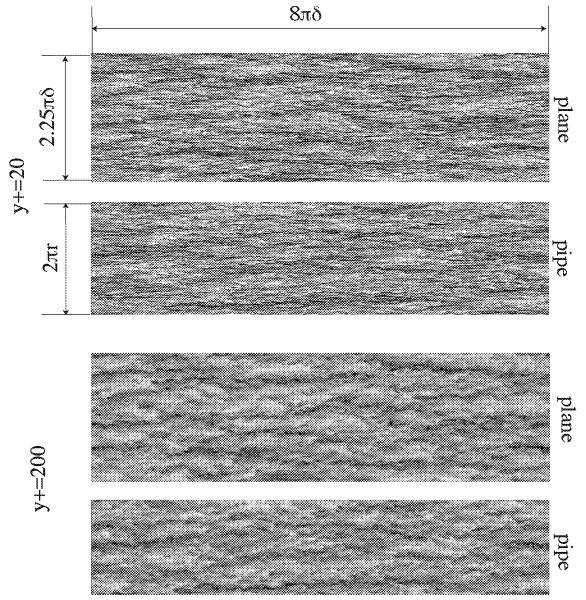


Figure 7: Instantaneous streamwise velocity fluctuations on an $x-z$ plane at $y^+ \sim 20$ and 200 at $Re_\tau = 1180$.

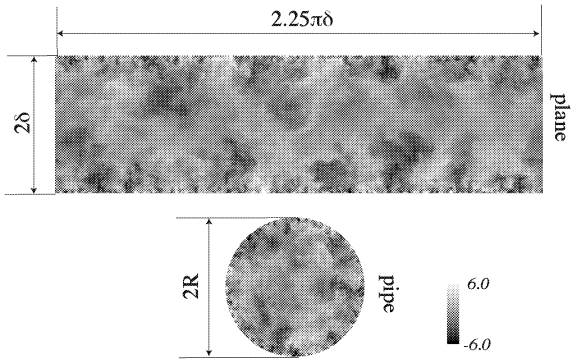


Figure 8: Instantaneous streamwise velocity fluctuations on a $y-z$ plane at $Re_\tau = 1180$

### Reynolds Number Scaling

The peak wavelengths of the plane channel at three different Reynolds numbers are plotted in Figs. 9 and 10. The streamwise energetic peak wavelengths collapse well by inner scaling near the wall which decay asymptotically to $\lambda_x^+ \sim 1000$, as seen in Fig. 9(a). They are constant in the buffer layer, then grow rapidly from $y^+ = 100$ to 200 in the log-law region until they reach $\lambda_x$ of around 3 to $12\delta$, but their collapse in the outer layer by outer units are only moderate. The spanwise peak wavelengths also show good collapse especially in the inner layer, as indicated in Fig. 10. In the near-wall region, they decay asymptotically to $\lambda_z^+ \sim 100$. It is acknowledged that this wavelength is the space between each sublayer streak, suggesting that the characteristic scale of streaks resulting from near-wall coherent structures is an universal phenomena. They grow in the buffer layer with good collapse in inner scaling, and reach constant values of $\lambda_z \sim 1.4\delta$ to $\sim 1.8\delta$ around $y^+ \sim 100$, which then collapse moderately well in outer scaling. From these figures, we can

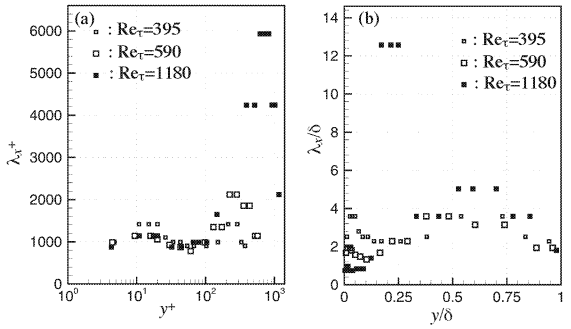


Figure 9: The streamwise peak wavelength of the premultiplied power spectra of *plane channel* flows: (a), *inner* scaling ($\lambda_x^+ < 6600$); (b), *outer* scaling.

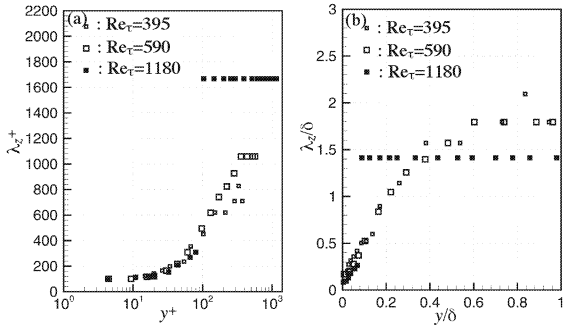


Figure 10: The spanwise/azimuthal peak wavelength of the premultiplied power spectra of *plane channel* flows: (a), *inner* scaling; (b), *outer* scaling.

say that the large structures obey the outer scaling and their spanwise size is about twice as large as the boundary layer thickness independent of the $Re$ range tested here.

### Difference between Plane Channel and Pipe Flows

To investigate the difference of the structures between channel and pipe flows, the peak wavelength of their premultiplied power spectra at $Re_\tau = 1180$ is indicated in Fig. 11. No significant difference can be found in the *inner* layer ($y+ < 100, y/\delta < 0.08$). Both channel and pipe flows have very large streamwise elongated structures ($\lambda_x/\delta \sim 12$) in the middle of log layer ($y^+ \sim 300, y/\delta \sim 0.25$), then they become smaller in the *outer* layer ($y/\delta \sim 0.4$), which is shown in Fig. 11(a). Compared with that of channel flow in the outer layer ($\lambda_x/\delta = 3 \sim 5$), the elongated structure is slightly smaller in pipe flow ($\lambda_x/\delta = 2 \sim 4$). The spanwise size of the corresponding large structures in channel flows maintains the same in or above the log layer, while the jagged profile of the pipe for the azimuthal peak wavelength is remarkable, which is indicated in Fig. 11(b).

### Azimuthal Structures

range tested here, which is shown in Fig. 12. We can explain the jagged pattern by plotting the energetic mode (peak of the premultiplied spectra) as the peak angle against the wall distance, and the pattern comes to be stepwise as indicated in Fig. 12(b). Here $\lambda_\theta$ is given as $2\pi/n$, in which $n$ is integer indicating the number of large scale structures allocated along azimuthal direction. In the Fig. 12(b), $\lambda_\theta$ is $2\pi/4$ below

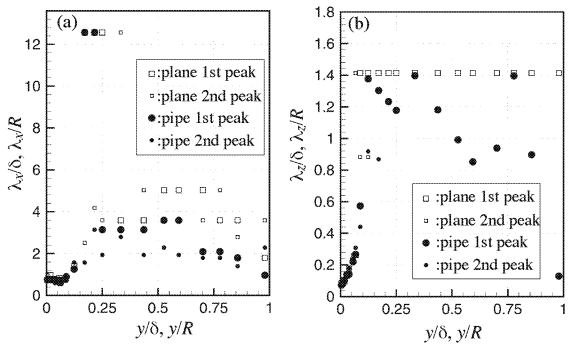


Figure 11: Comparison of the peak wavelength of the premultiplied power spectra between *channel* and *pipe* flows at $Re_\tau = 1180$ in *outer* scaling: (a), streamwise; (b), spanwise.

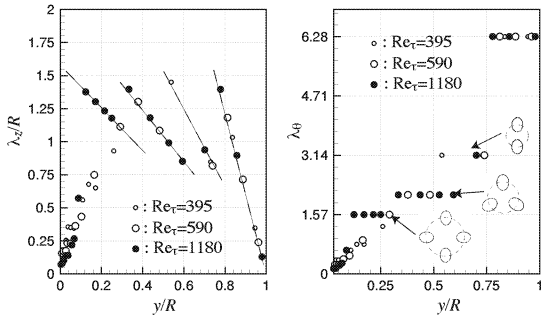


Figure 12: The azimuthal peak (a)wavelength/(b)angle of the premultiplied power spectra of *pipe* flows.

$y/R = 0.3$, $2\pi/3$ at $y/R = 0.3 \sim 0.6$, $2\pi/2$ at $y/R = 0.6 \sim 0.8$, and $2\pi/1$ above $y/R = 0.8$. It is important to note here that at the position where shift of the azimuthal number of the large structures occurs, the azimuthal spacing of each structure can recover $1.4R$, such as $y/R = 0.3$ where the azimuthal spacing of three structures is $2\pi \times 0.7R/3 \sim 1.5$ and $y/R = 0.6$ where the spacing of two structures is $2\pi \times 0.4R/4 \sim 1.3$. As indicated in Fig. 11(b), the characteristic spanwise spacing of the large structures in channel flow is $1.4\delta$ in and above the log layer, the lateral spacing of 1.4 times the boundary thickness may be a universal feature of the wall turbulence in the outer layer.

## CONCLUSIONS

The findings of the present study can be summarised as follows: An unexpectedly fine grid spacing of $h_x^+ \sim 30$ and $h_z^+ \sim 20$ in the streamwise and spanwise directions is required to properly capture the 1-D premultiplied power spectrum and its peak at the lower wavenumber in the outer layer where large scales remarkably appear. This result indicates an apparent strong relation between the near-wall small scales and the large scales in the outer layer; In the *inner* layer of both channel and pipe flows, the streamwise and spanwise peak wavelength of the premultiplied spectra collapse very well near the wall in inner scaling, which indicates that there is not remarkable difference of the near-wall feature between channel and pipe flows; In the log layer around $y^+ \sim 300$ of both channel and pipe flows at $Re_\tau = 1180$, *very* large streamwise elongated structures of the size comparable to the half of the numerical domain ($8\pi$ times the channel half-height or the radius of the pipe) exist, which may indicate still larger domain size is required: In the *outer* layer above $y/\delta = 0.3$, rather smaller large structures than in the log layer exist, but their streamwise size is slightly smaller in pipe flow ($\lambda_x/R = 2 \sim 4$) than those in channel flow ($\lambda_x/\delta = 3 \sim 5$). The spanwise/azimuthal spacing of the large structures may be independent on the Reynolds number, and is stable at $\lambda_z/\delta$ or $\lambda_z/R = 1.4$.

## ACKNOWLEDGEMENTS

This work has been supported in part by a Grant-in -Aid for Scientific Research from the Ministry of Education, Science, Sorts and Culture of Japan (No. 14750110). We are also indebted to Dr. Y. Morinishi for his providing the simulation code used here.

## REFERENCES

DeGraaff, D. B., and Eaton, J. K., 2000, "Reynolds-number scaling of the flat-plate turbulent boundary layer", *J. Fluid Mech.*, Vol. 422, pp. 319.

Del Álamo, J. C., and Jiménez, J., 2001, "Direct numerical simulation of the very large anisotropic scales in a turbulent channel", *Center for Turbulence Research Annual Research Briefs, Stanford University*, pp. 329.

Del Álamo, J. C., and Jiménez, J., 2003, "Spectra of the very large anisotropic scales in turbulent channels", *Phys. Fluids*, Vol. 15, pp. L41.

Dukowicz, J. K., and Dvinsky, A. S., 1992 "Approximation as a higher order splitting for the implicit incompressible flow equations", *J. Comput. Phys.*, Vol. 102, pp. 334.

Germano, M., Piomelli, U., Moin, P., and Cabot, W. C., 1991, "A dynamic subgrid-scale eddy viscosity model", *Phys. Fluids*, Vol. A3, pp. 1760.

Kim, K. C., and Adrian, R. J., 1999, "Very large-scale motion in the outer layer", *Phys. Fluids*, Vol. 11, pp. 417.

Morinishi, Y., Lund, T. S., Vasilyev, O. V., and Moin, P, 1998, "Fully conservative higher order finite difference schemes for incompressible flow", *J. Comp. Phys.*, Vol. 142, pp. 1.

Morinishi, Y., Vasilyev, O. V., and Ogi, T., 2004, "Fully conservative finite difference scheme in cylindrical coordinates for incompressible flow simulations", *J. Comp. Phys.*, Vol. 197, pp. 484.

Morrison, J. J., Jiang, W., McKeon, B. J., and Smits, A. J., 2002, "Reynolds number dependence of streamwise velocity spectra in turbulent pipe flow", *Phy. Rev. Lett.*, Vol. 88, pp. 214501.

Perry, A. E., Henbest, S., and Chong, M. S., 1986, "A theoretical and experimental study of wall turbulence", *J. Fluid Mech.*, Vol. 165, pp. 199.

Tsubokura, M., 2001, "Proper representation of the subgrid-scale eddy viscosity for the dynamic procedure in large eddy simulation using finite difference method", *Phys. Fluids*, Vol. 13, pp. 500.